Supplementary Material

Discerning the magnetization reversal mechanism and magnetic interactions in arrays of FeNi nanowires

Alonso J. Campos-Hernández, Ester M. Palmero* and Alberto Bollero§

Group of Permanent Magnets and Applications, IMDEA Nanoscience, 28049 Madrid, Spain

*Corresponding author (E.M. Palmero) - Email: ester.palmero@imdea.org

1 Raw energy dispersive X-ray spectroscopy (EDS/EDX) spectra

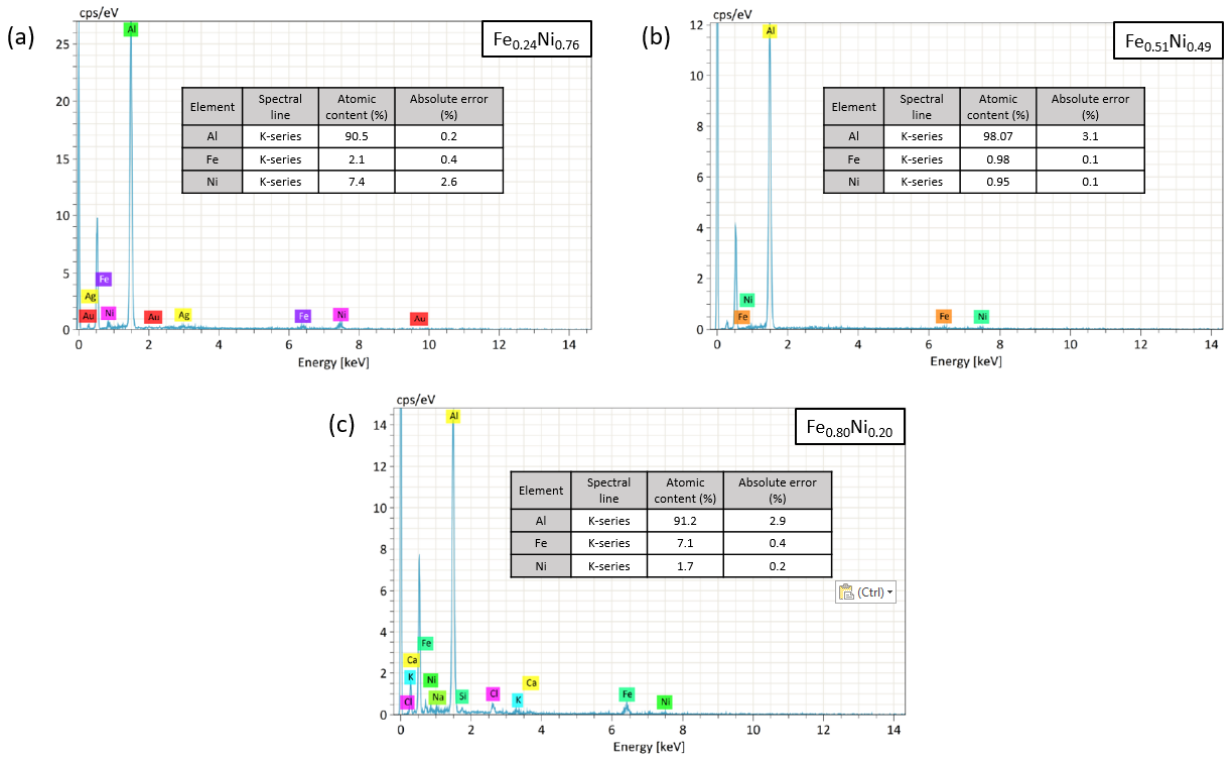

Figure 1. *EDX spectra for samples grown at -1.1V vs the reference electrode with electrolytes with a) 23% Fe, b) 50% Fe and c) 75% Fe. Each subfigure includes its corresponding chemical quantification table, and the top-right labels in each subfigures indicate the corresponding measured nanowire composition.*

§Present address (A. Bollero): Advanced Technologies and Micro Systems, Robert Bosch GmbH, Corporate Sector Research, Renningen, 70465 Stuttgart, Germany
Email: Alberto.Bollero@de.bosch.com

2 Modeling of magnetization reversal in cylindrical nanowires

There are three main magnetization reversal modes in magnetic nanowires [1]: coherent rotation (mode C), the classic Stoner-Wohlfarth model where all spins rotate simultaneously [2]; transverse wall propagation (mode T), where a transverse domain wall is nucleated and expands through the nanowire [2]; and vortex wall propagation (mode V) or "curling" mode [3], where a vortex domain wall is nucleated and propagates.

The presence of one reversal mechanism or another will depend on both the properties of the nanowire alloy (magnetization saturation, exchange length, etc.) and of the nanowire geometry (nanowire length, diameter, etc.). Each reversal mode will create a different dependence of the coercivity with the angle θ between the nanowire axis and the applied field, and therefore angular measurements can be used to distinguish between the mechanisms.

For both the coherent rotation and transverse wall modes, the nucleation field H_n (at which reversal starts) is given by [1]

$$H_n^x(\theta) = \frac{2\,K_t(x)\sqrt{1-t^2+t^4}}{\mu_0 M_s^2(1+t^2)} M_s \tag{1}$$

with $x = C, T$; $t = \tan(\theta)^{1/3}$ and where $K_t(x)$ is the total magnetic anisotropy of the sample, which does however depend on the magnetization reversal mode being considered. Note that, within this model, the nucleation field is taken to be equal to the coercivity ($H_n = H_c$).

This anisotropy constant includes several contributions, so that [4]

$$K_t(x) = K_{sh}(x) + K_{ms} + K_{mc} + K_{me} \tag{2}$$

where $K_{sh}(x)$ is the shape anisotropy and depends on the magnetization reversal mode considered, K_{ms} is the magnetostatic contribution to the anisotropy stemming from the magnetic alignment of the nanowires, K_{mc} is the magnetocrystalline anisotropy and K_{me} is the magnetoelastic contribution. Due to the near-one-dimensional nature of the nanowires, the shape anisotropy tends to be the dominant contribution to the total, followed by the magnetostatic and magnetocrystalline terms [4].

For the two main anisotropy contributions considered, we should note that K_{ms} grows with the saturation magnetization M_s, while for the shape anisotropy we have

$$K_{sh}(x) = \frac{1}{4}\mu_o M_s^2(1 - 3N_z(l(x))) \tag{3}$$

$N_z(l(x))$ is the demagnetization factor along the nanowire axis, and the length $l(x)$ considered is the total length of the nanowire L_{NW} in the case of reversal mode C and the transverse domain wall width ω_T in the case of reversal mode T [1].

The demagnetization factors are given as a function of the nanowire aspect ratio $m = {}^{L_{NW}}/_{r}$. For nanowires of sufficient aspect ratio ($m > 10$, as is our case), $N_z(L_{NW}) \sim 0$ [5]. For nanowires of a general length and prolate form (i.e. $m > 1$) the demagnetization factors in the axial (N_z) and perpendicular directions (N_x, N_y) are given by [5]:

$$N_z(m) = 4\pi \frac{1}{2(m^2-1)}\left[\frac{m}{2(m^2-1)^{\frac{1}{2}}} \ln\frac{m+(m^2-1)^{\frac{1}{2}}}{m-(m^2-1)^{\frac{1}{2}}} - 1\right] \quad (4)$$

$$N_x(m) = N_y(m) = 4\pi \frac{m}{2(m^2-1)}\left[m - \frac{1}{2(m^2-1)^{\frac{1}{2}}} \ln\frac{m+(m^2-1)^{\frac{1}{2}}}{m-(m^2-1)^{\frac{1}{2}}}\right] \quad (5)$$

These formulae can then be applied to the transverse domain wall widths ω_T to find the necessary demagnetization factors for Eq. (3) and mode T. Considering together all this, we can finally calculate the angular-dependent coercivity of Eq. (1) for the coherent rotation (C mode) and transverse wall (T mode) magnetization reversal modes by taking the $K_{ms} + K_{mc} + K_{me}$ sum as a fit parameter. For vortex wall (V mode) magnetization reversal, the angular dependence of H_c was given in [3] for both when there is a magnetocrystalline anisotropy and when there is none. In the case of neglecting the magnetocrystalline anisotropy, we have

$$H_c(\theta) = 2\pi M_s \left| \frac{(2N_z - {}^{k}/_{S^2})(2N_x - {}^{k}/_{S^2})}{\sqrt{(2N_z - {}^{k}/_{S^2})^2 \sin^2\theta + (2N_x - {}^{k}/_{S^2})^2 \cos^2\theta}} \right| \quad (6)$$

where $S = r/r_0$ with $r_0 = A^{1/2}/M_s$ and $k = q^2/\pi$ (q is the smallest solution of the Bessel functions and is 1.8412 for a cylinder).

By comparing the angular curves of coercivity for each magnetization reversal mode with the best-fit value of $K_t(x)$, we can deduce the leading reversal mechanism in each case, as the system will follow the path of lowest energy, i.e., the reversal mechanism with the lowest coercivity values.

The angular coercivity values of the studied samples can be found in Fig. 5 in the main manuscript, along with their best-fit curves for each reversal mode. The parameters of Fe and Ni (the saturation magnetization M_s, and the exchange length A_{ex}) necessary for performing the calculations were taken from [6]–[8]. The transverse domain wall lengths of our samples (necessary to calculate K_{sh} in the transverse domain wall case) were estimated from the micromagnetic simulation results provided in [9] as being 65, 35, 32, 28 and 28 nm respectively for the Ni, $Fe_{0.24}Ni_{0.76}$, $Fe_{0.51}Ni_{0.49}$, $Fe_{0.80}Ni_{0.20}$ and Fe samples respectively, by taking into account their M_s and diameter.

3 NW coercivity angular measurements

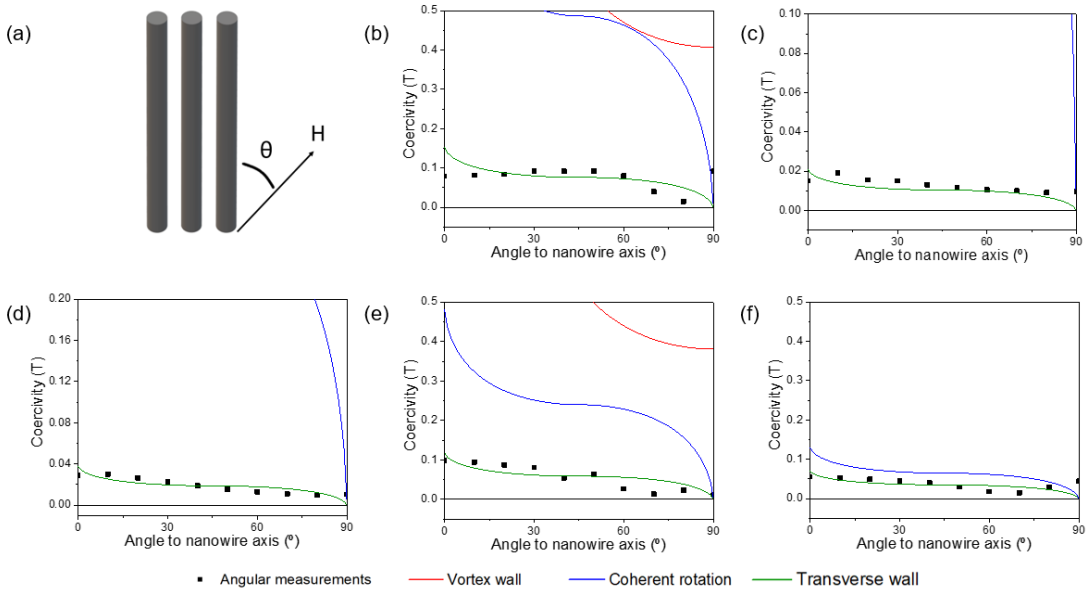

Figure 2. *(a) Diagram sketching the angular measurements performed and (b)-(f) coercivity measured at different angles to the NWs axis and fits to magnetization reversal models for the arrays of NWs with the following composition: (b) Fe, (c) $Fe_{0.80}Ni_{0.20}$, (d) $Fe_{0.51}Ni_{0.49}$, (e) $Fe_{0.24}Ni_{0.76}$, and (f) Ni. Coercivity angular measurement plots have been zoomed-in as necessary in each case to be able to appreciate the coercivity angular evolution.*

4 First-order reversal curve (FORC) marginal coercivity distributions

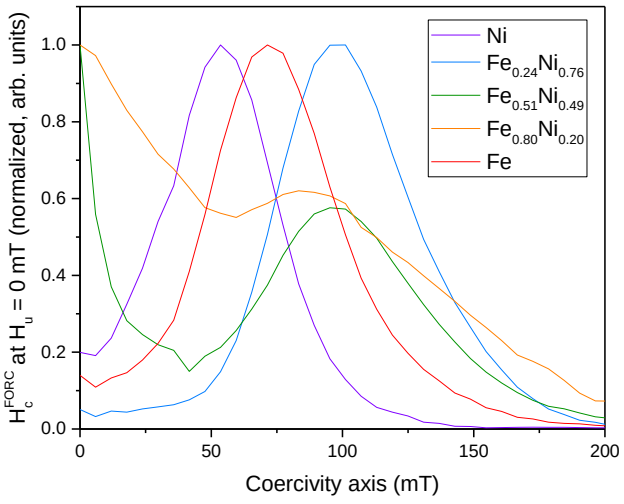

Figure 3. *FORC marginal coercivity distributions for the samples studied. The y-axis indicates the FORC intensity, with the values of each data series normalized to its maximum value, while the x-axis is the coercivity axis of the FORC diagram.*

References

[1] L. G. Vivas *et al.*, 'Magnetic anisotropy in CoNi nanowire arrays: analytical calculations and experiments', *Phys. Rev. B*, vol. 85, no. 3, p. 035439 (2012), doi: 10.1103/PhysRevB.85.035439.

[2] R. Lavín, J. C. Denardin, J. Escrig, D. Altbir, A. Cortés, and H. Gómez, 'Angular dependence of magnetic properties in Ni nanowire arrays', *J. Appl. Phys.*, vol. 106, no. 10, p. 103903 (2009), doi: 10.1063/1.3257242.

[3] A. Aharoni, 'Angular dependence of nucleation by curling in a prolate spheroid'. *J. Appl. Phys.*, vol. 82, no. 3, pp. 1281–1287 (1997), doi: 10.1063/1.365899.

[4] O. Dragos *et al.*, 'Anomalous codeposition of *fcc* NiFe nanowires with 5–55% Fe and their morphology, crystal structure and magnetic properties," *J. Electrochem. Soc.*, vol. 163, no. 3, pp. D83–D94 (2015), doi: 10.1149/2.0771603jes.

[5] L. Sun *et al.*, 'Tuning the properties of magnetic nanowires', *IBM J. Res. Dev.*, vol. 49, no. 1, pp. 79–102 (2005), doi: 10.1147/rd.491.0079.

[6] H. Okamoto, *Phase diagrams of binary iron alloys*. Materials Park, Ohio, USA: The Materials Information Society, 1993.

[7] A. Michels *et al.*, 'Exchange-stiffness constant in cold-worked and nanocrystalline Ni measured by elastic small-angle neutron scattering', *J. Appl. Phys.*, vol. 87, no. 9, pp. 5953–5955 (2000), doi: 10.1063/1.372577.

[8] C. Bran *et al.*, 'Correlation between structure and magnetic properties in Co_xFe_{100-x} nanowires: the roles of composition and wire diameter', *J. Phys. D: Appl. Phys.*, vol. 48, no. 14, p. 145304 (2015), doi: 10.1088/0022-3727/48/14/145304.

[9] R. Moreno *et al.*, 'Detailed examination of domain wall types, their widths and critical diameters in cylindrical magnetic nanowires', *J. Magn. Magn. Mater.*, vol. 542, p. 168495 (2022), doi: https://doi.org/10.1016/j.jmmm.2021.168495.